Calculation of optical forces on an ellipsoid using vectorial ray tracing method

Jin-Hua Zhou,[1,2] Min-Cheng Zhong,[1] Zi-Qiang Wang,[1] and Yin-Mei Li[1,2,*]

[1]*Department of Optics and Optical Engineering, University of Science and Technology of China, Hefei, Anhui, 230026, China*

[2]*Hefei National Laboratory for Physical Sciences at the Microscale, Hefei, Anhui, 230026, China*

[*]*liyinmei@ustc.edu.cn*

Abstract: For a triaxial ellipsoid in an optical trap with spherical aberration, the optical forces, torque and stress are analyzed using vectorial ray tracing. The torque will automatically regulate ellipsoid's long axis parallel to optic axis. For a trapped ellipsoid with principal axes in the ratio 1:2:3, the high stress distribution appears in x-z plane. And the optical force at x-axis is weaker than at y-axis due to the shape size. While the ellipsoid departs laterally from trap center, the measurable maximum transverse forces will be weakened due to axial equilibrium and affected by inclined orientation. For an appropriate ring beam, the maximum optical forces are strong in three dimensions, thus, this optical trap is appropriate to trap cells for avoiding damage from laser.

OCIS codes: (350.4855) Optical tweezers or optical manipulation; (080.5692) Ray trajectories in inhomogeneous media.

References and links

1. J. G. Wu, Y. M. Li, D. Lu, Z. Liu, Z. D. Cheng, and L. Q. He, "Mesurement of the membrane elasticity of red blood cell with osmotic pressure by optical tweezers," Cryo Lett. **30**, 89–95 (2009).
2. S. Bayoudh, T. A. Nieminen, N. R. Heckenberg, and H. Rubinsztein-Dunlop, "Orientation of biological cells using plane-polarized Gaussian beam optical tweezers," J. Mod. Opt. **50**, 1581–1590 (2003).
3. G. Volpe, G. P. Singh, and D. Petrov, "Dynamics of a growing cell in an optical trap," Appl. Phys. Lett. **88**(23), 231106 (2006).
4. D. P. Cherney, T. E. Bridges, and J. M. Harris, "Optical trapping of unilamellar phospholipid vesicles: investigation of the effect of optical forces on the lipid membrane shape by confocal-Raman microscopy," Anal. Chem. **76**(17), 4920–4928 (2004).
5. J. C. Loudet, A. G. Yodh, and B. Pouligny, "Wetting and contact lines of micrometer-sized ellipsoids," Phys. Rev. Lett. **97**(1), 018304 (2006).
6. Y. Harada and T. Asakura, "Radiation forces on a dielectric sphere in the Rayleigh scattering regime," Opt. Commun. **124**(5-6), 529–541 (1996).
7. L. Novotny, R. X. Bian, and X. S. Xie, "Theory of nanometric optical tweezers," Phys. Rev. Lett. **79**(4), 645–648 (1997).
8. K. F. Ren, G. Gréhan, and G. Gouesbet, "Prediction of reverse radiation pressure by generalized Lorenz-Mie theory," Appl. Opt. **35**(15), 2702–2710 (1996).
9. T. A. Nieminen, H. Rubinsztein-Dunlop, N. R. Heckenberg, and A. I. Bishop, "Numerical modeling of optical trapping," Comput. Phys. Commun. **142**(1-3), 468–471 (2001).
10. F. Xu, K. F. Ren, G. Gouesbet, X. S. Cai, and G. Gréhan, "Theoretical prediction of radiation pressure force exerted on a spheroid by an arbitrarily shaped beam," Phys. Rev. E Stat. Nonlin. Soft Matter Phys. **75**(2), 026613 (2007).
11. S. H. Simpson and S. Hanna, "Optical trapping of spheroidal particles in Gaussian beams," J. Opt. Soc. Am. A **24**(2), 430–443 (2007).
12. T. A. Nieminen, V. L. Y. Loke, A. B. Stilgoe, G. Knoner, A. M. Branczyk, N. R. Heckenberg, and H. Rubinsztein-Dunlop, "Optical tweezers computational toolbox," J. Opt. Soc. Am. A **9**(8), S196–S203 (2007).
13. S. H. Simpson and S. Hanna, "Computational study of the optical trapping of ellipsoidal particles," Phys. Rev. A **84**(5), 053808 (2011).
14. Z. J. Li, Z. S. Wu, and Q. C. Shang, "Calculation of radiation forces exerted on a uniaxial anisotropic sphere by an off-axis incident Gaussian beam," Opt. Express **19**(17), 16044–16057 (2011).
15. J. P. Barton, D. R. Alexander, and S. A. Schaub, "Internal fields of a spherical particle illuminated by a tightly focused laser beam: Focal point positioning effects at resonance," J. Appl. Phys. **65**(8), 2900–2906 (1989).

#167000 - $15.00 USD Received 18 Apr 2012; revised 23 May 2012; accepted 5 Jun 2012; published 19 Jun 2012

16. A. Ashkin, "Forces of a single-beam gradient laser trap on a dielectric sphere in the Ray Optics Regime," Biophys. J. **61**(2), 569–582 (1992).
17. R. C. Gauthier, "Theoretical investigation of the optical trapping force and torque on cylindrical micro-objects," J. Opt. Soc. Am. B **14**(12), 3323–3333 (1997).
18. K. Shima, R. Omori, and A. Suzuki, "Forces of a single-beam gradient-force optical trap on dielectric spheroidal particles in the geometric-optics regime," Jpn. J. Appl. Phys. **37**(Part 1, No. 11), 6012–6015 (1998).
19. J. S. Kim and S. W. Kim, "Dynamic motion analysis of optically trapped nonspherical particles with off-axis position and arbitrary orientation," Appl. Opt. **39**(24), 4327–4332 (2000).
20. D. H. Li, J. X. Pu, and X. Q. Wang, "Radiation forces of a dielectric medium plate induced by a Gaussian beam," Opt. Commun. **285**(7), 1680–1683 (2012).
21. J. H. Zhou, H. L. Ren, J. Cai, and Y. M. Li, "Ray-tracing methodology: application of spatial analytic geometry in the ray-optic model of optical tweezers," Appl. Opt. **47**(33), 6307–6314 (2008).
22. P. B Bareil, Y. L. Sheng, and A. Chiou, "P. B Bareil, Y. L. Sheng, and A. Chiou, "Local scattering stress distribution on surface of a spherical cell in optical stretcher," Opt. Express **14**(25), 12503–12509 (2006).
23. M. Born and E. Wolf, "Reflectivity and transmissivity," in *Principles of Optics* (Cambridge University Press, 1999).
24. E. Aspnes, T. D. Milster, and K. Visscher, "Optical force model based on sequential ray tracing," Appl. Opt. **48**(9), 1642–1650 (2009).
25. X. Sheng-Hua, L. Yin-Mei, and L. Li-Ren, "Systematical study of the trapping forces of optical tweezers formed by different types of optical ring beams," Chin. Phys. **15**(6), 1391–1397 (2006).
26. P. Liu and B. Lu, "Phase singularities of the transverse field component of high numerical aperture dark-hollow Gaussian beams in the focal region," Opt. Commun. **272**(1), 1–8 (2007).
27. S. H. Xu, Y. M. Li, and L. R. Lou, "Axial optical trapping forces on two particles trapped simultaneously by optical tweezers," Appl. Opt. **44**(13), 2667–2672 (2005).
28. P. B. Bareil, Y. Sheng, Y. Q. Chen, and A. Chiou, "Calculation of spherical red blood cell deformation in a dual-beam optical stretcher," Opt. Express **15**(24), 16029–16034 (2007).
29. M. Gu, P. C. Ke, and X. S. Gan, "Trapping force by a high numerical-aperture microscope objective obeying the sine condition," Rev. Sci. Instrum. **68**(10), 3666–3668 (1997).
30. P. Török, P. Varga, Z. Laczik, and G. R. Booker, "Electromagnetic diffraction of light focused through a planar interface between materials of mismatched refractive-indexes - an integral-representation," J. Opt. Soc. Am. A **12**(2), 325–332 (1995).
31. F. Merenda, G. Boer, J. Rohner, G. Delacrétaz, and R. P. Salathé, "Escape trajectories of single-beam optically trapped micro-particles in a transverse fluid flow," Opt. Express **14**(4), 1685–1699 (2006).
32. Z. Gong, Z. Wang, Y. M. Li, L. R. Lou, and S. H. Xu, "Axial deviation of an optically trapped particle in trapping force calibration using the drag force method," Opt. Commun. **273**(1), 37–42 (2007).

1. Introduction

In many applications of optical tweezers, there were some irregular trapped particles, such as red blood cells (RBCs) [1], chloroplasts [2], growing yeast cells [3] and phospholipid vesicles [4].Those nonspherical particles can be regarded as spheroids or triaxial ellipsoids. To investigate wetting problem for ellipsoids, the ellipsoids can be levitated to a water-air interface by optical trap [5].The analysis of forces on an ellipsoid will help us understand dynamic behavior of irregular particle in an optical trap.

Generally, there are three approaches for theoretically calculating optical forces for a particle in an optical trap. The Rayleigh particle can be regarded as a dipole in electromagnetic field, and it suffers optical forces due to nonuniform field distribution [6, 7]. While the particle size varies from submicron to several microns, the interaction between particle and electromagnetic field will disturb field distribution, so the optical forces need to be calculated with various electromagnetic (EM) models [8–15]. For large size particle, the interaction between particle and field can be simplified in refraction and reflection, i.e., the forces can be calculated in ray-optics (RO) regime [16–21].

In the previous investigations, there were some theoretical methods for calculating optical forces and torque on a nonspherical particle by means of symmetry. Using T-matrix method Nieminen et al. [9]calculated optical forces of spheroidal and cylindrical particles with different aspect ratios. For an arbitrarily beam, Xu et al. [10] analyzed the optical forces using EM model. Simpson and Hanna [11] detailed the calculation of optical forces and torque on spheroid by a Gaussian beam. Using RO model Shima et al. [18] indicated that a spheroid with prolate orientation has more axial stability than oblate orientation. Recently, Li et al.

#167000 - $15.00 USD Received 18 Apr 2012; revised 23 May 2012; accepted 5 Jun 2012; published 19 Jun 2012

[20] calculated the radiation forces on a dielectric plate by a Gaussian beam. Those results indicated the optical forces were related with particle shape and orientation.

For a triaxial ellipsoid, there are some difficulties to describe the forces by some simple formulas due to its non-symmetry. Recently, a discrete dipole approximation (DDA) method is used to calculate the stiffness of ellipsoidal particles with different size or shape [13]. However, it is unclear for characteristics of a triaxial ellipsoid in different optical traps. As an approximation approach, RO model cannot reflect the effects of diffraction by a high numerical aperture objective and resonance between the field and the microparticle, but it is a very simple and valid method compared with the EM model. Based on vectorial ray tracing [21] and rotating coordinates, we calculate the forces, torque and stress on a trapped ellipsoid under an optical trap with spherical aberration at a glass-water interface. Furthermore, the effects of beam profile and particle orientation on optical forces are analyzed.

2.Vectorial ray tracing

The force of a single ray on a sphere was described by Ashkin [16]. For tracing a single ray striking a triaxial ellipsoid, the incident angles of reflection and refraction will vary with striking location. And so does the incident plane. Thus, the force needs to be calculated in every incident plane.

2.1. Force on an interface

When photons get through an interface, their moment is changed by the reflection and refraction. This will induce a force on the interface due to momentum conservation. While photons go across a medium with he dielectric refractive index n_m to other medium with refractive index n_p, the force on this interface is express as [22]

$$\mathbf{F} = \frac{P}{c}[n_p T\ \cos\gamma - n_m \cos\theta(1+R)]\mathbf{n}, \tag{1}$$

where P is power, θ and γ are the incident and refractive angles, respectively, R and T are Fresnel reflection and transmission coefficients of energy flow [23], the unit vector **n** denotes interface surface normal towards n_m. The force can be described by trapping efficiency Q, which is a dimensionless factor of $Q = Fc / n_m P$.

2.2. Beam profile

In the process of ray tracing, a focused beam in the plane of an objective entrance aperture is generally divided into many rays. The intensity of each single ray varies with location in this plane owing to non-uniform beam profile. In RO model, the uniform amplitude [16], Gaussian beam profile [21, 24] and ring beam [25] have been reported. Here, we will take a formula to describe the Gaussian and ring beams. The intensity of electrical field can be described as below [26]

$$E_x(r) = A(\frac{r^2}{\omega_0^2})^n \exp(-\frac{r^2}{\omega_0^2}), \qquad n = 0,1,2,\cdots, \tag{2}$$

where $A = \sqrt{\frac{P 2^{2n+2}}{(2n)!\pi\omega_0 n_m \varepsilon_0 c}}$, n is the beam order, ω_0 is the beam waist width. The Gaussian beam and ring beam can be described as $n = 0$ and $n > 0$, respectively. So the power of surface element Δs can be written as

#167000 - $15.00 USD Received 18 Apr 2012; revised 23 May 2012; accepted 5 Jun 2012; published 19 Jun 2012

$$\Delta P = \frac{P 2^{2n+1}}{2n!\pi\omega_0^2}(\frac{r^2}{\omega_0^2})^{2n} \exp(-\frac{2r^2}{\omega_0^2})\Delta s. \tag{3}$$

2.3Vectorial ray tracing for an ellipsoid

There were some reports of ray tracing in some cases: calculating optical forces on a spherical bead [21], a cylindrical particle [17], a spheroid [18], a plate [20] and two beads [27]; calculating stress on RBCs [22, 28] and ray tracing by commercial software [24]. Here, we introduce a method to trace the reflection and refraction of a single ray striking an ellipsoid by vectors.

A focused single ray strikes a triaxial ellipsoid in a Cartesian coordinate system based on the focus of an objective as original point *O* and the objective optic axis as *z*-axis, as shown in Fig. 1(a). The center of ellipsoid is located at $P(x_0,y_0,z_0)$. The objective entrance aperture is in the O_0 plane, where R_{obj} is the radius of entrance aperture, f_{obj} is the objective focus length. When a single ray located at (r,β_0) in the O_0 plane is deflected by the objective, the ray meets the relation of $\sin\alpha_1 = r / f_{obj}$ since the objective obeys the sine condition [29]. Due to spherical aberration of refractive index mismatch in an interface between glass(n_g) and water(n_w), the actual incident ray is further deflected in the interface and goes across a point $G(0,0,\Delta z)$. The direction of the incident ray striking the ellipsoid is described as the unit vector

$$\mathbf{n}_1(n_{1x}, n_{1y}, n_{1z}) = (-\sin\alpha_2\cos\beta_0, -\sin\alpha_2\sin\beta_0, \cos\alpha_2), \tag{4}$$

where the angle $\alpha_2$meets Snell's law of $n_g\sin\alpha_1 = n_w\sin\alpha_2$. In those relationships, $f_{obj} = n_g R_{obj} / NA$, where *NA* is the numerical aperture of an objective. The deviation Δz varies with a depth z_{cg}, which indicates the distance from trap center to coverslip. According to geometric relations,

$$\Delta z = z_{cg} + \left| z_{cg} \right| \tan\alpha_1 / \tan\alpha_2. \tag{5}$$

The incident ray is described as a linear equation by means of the position of point *G* and vector $\mathbf{n}_1$. So the position of the first incident point can be solved with the standard equation of an ellipsoid and a linear equation of incident ray.

#167000 - $15.00 USD Received 18 Apr 2012; revised 23 May 2012; accepted 5 Jun 2012; published 19 Jun 2012

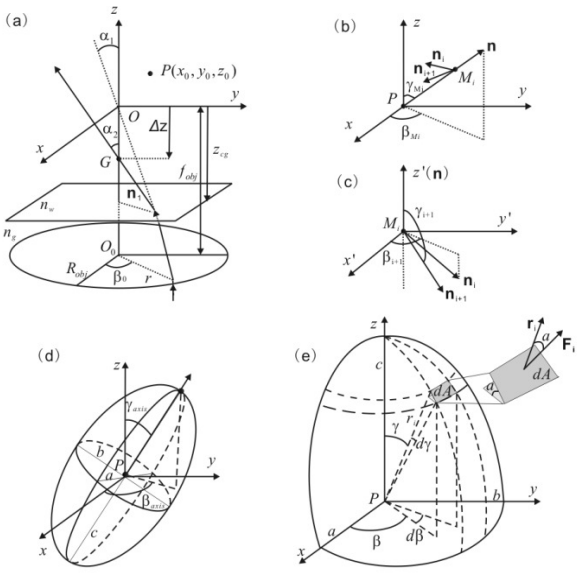

Fig. 1. Tracing a single ray striking an ellipsoid. $P(x_0, y_0, z_0)$ is the center of the ellipsoid. M_i is the i-th incident point of the ray striking ellipsoid. Length a, b and c indicate the semi-principal axes. (a) Scheme of the ray ($\mathbf{n}_1$) deflected by an objective with spherical aberration; (b) Spatial orientation of incident ray $\mathbf{n}_i$, reflective ray $\mathbf{n}_{i+1}$ and outward normal $\mathbf{n}$ for the i-th incident point M_i; (c) The vectors in (b) after rotating coordinate system with $\mathbf{n}$ as z'-axis; (d) An ellipsoid with the arbitrary orientation (β_{ell}, γ_{ell}); (e) Spatial orientation of a surface element of dA, $(\mathbf{F})_i$ is the total force on this surface element.

After a single ray striking an ellipsoid, the last reflective ray is regarded as the next incident ray, and each incident point can be determined by equations of the new incident ray and ellipsoid. While an ellipsoid centered at the origin point O and each semi-principal axis (a,b,c) is parallel to coordinate axis, as shown in Fig. 1(b), the i-th incident point $M_i\left(x_i, y_i, z_i\right)$ and incident ray $\mathbf{n}_i\left(n_{ix}, n_{iy}, n_{iz}\right)$ meet the Eq. (6).

$$\frac{x^2}{a^2}+\frac{y^2}{b^2}+\frac{z^2}{c^2}=1, \tag{6A}$$

$$\frac{x-x_i}{n_{ix}}=\frac{y-y_i}{n_{iy}}=\frac{z-z_i}{n_{iz}}=t. \tag{6B}$$

The vector $\mathbf{n}$ indicates the outward normal of the interface at M_i. By solving the parameter t, the position M_i and $\mathbf{n}\left(\beta_{M_i}, \gamma_{M_i}\right)$ are determined. According to $\mathbf{n}_i$ and $\mathbf{n}$, both the incident and refractive angles can be calculated at M_i. The force at M_i can be calculated using Eq. (1).Since the reflective ray $\mathbf{n}_{i+1}$ is in the incident plane, the orientation of vector $\mathbf{n}_{i+1}(\beta_{i+1}, \gamma_{i+1})$ can be easily determined by incident angle and $\mathbf{n}_i$ after rotating coordinate system with the normal $\mathbf{n}$ as z'-axis (see in Fig. 1(c)). Then vector $\mathbf{n}_{i+1}$ is finally determined by inversing coordinate system. Then the next incident point and corresponding force can be calculated by repeating previous process.

When the center of ellipsoid deviates from optic axis, the vector $\mathbf{n}_i$ and position M_i can be also calculated by mean of coordinate translation. If the semi-principal axes of ellipsoid are inclined to an arbitrary orientation (β_{axis}, γ_{axis}) (in Fig. 1(d)), we can calculate force in a new coordinate system by rotating the semi-principal axes parallel to coordinate axes. The final force is the summation of inversed force at each incident point.

#167000 - $15.00 USD Received 18 Apr 2012; revised 23 May 2012; accepted 5 Jun 2012; published 19 Jun 2012

2.4. Senkrecht and parallel components of a single ray

In RO model, the power ratios of the senkrecht and parallel components (s- and p-components) are the same in the circularly polarized or random polarized states, i.e., $f_s = f_p = 0.5$. For a linear polarized beam, the power ratio can be determined by the intersection angle between the polarized direction at incident point and the normal of incident plane [21]. While a ray gets through an interface, the intensity of s- and p-components will vary with incident angle, which was detailed in the reference [30].

If the electric field **E** indicates the direction and intensity of a single ray after a reflection or refraction from an interface, the polarization vector $\mathbf{n}_\mathrm{p} = \mathbf{E}/|\mathbf{E}|$. Since the incident ray $\mathbf{n}_\mathrm{i}$ and the interface normal **n** compose the incident plane, the normal of which can be expressed as $\mathbf{n}_{inci} = \mathbf{n} \times \mathbf{n}_\mathrm{i}$. The power ratio of s-component $f_s = \cos^2 \Omega$, which Ω meets $\cos\Omega = \mathbf{n}_p \bullet \mathbf{n}_{inci}$. Accordingly, $f_p = 1 - f_s$ for the p-component. The power of the single ray decreases with many times of reflection and refraction. Before depletion of the ray, f_s and f_p will vary with incident point.

2.5. Stress and torque

The force rapidly varies with position on the surface of ellipsoid. To demonstrate this characteristic, the stress is introduced to record force per unit area. The ellipsoidal surface elements are hardly divided into the same area, but it is easy to divide the surface of ellipsoid into grids by orientation angle (β, γ,). If the distance from a surface element to the center is r_i (Fig. 1(e)), the area of reference sphere with radius r_i can be expressed as $r_i^2 d\beta d\gamma$. Here the sign *i* indicates the i-th surface element. Since there is an intersection angle of αbetween the normal of ellipsoidal surface element and the normal of spherical surface element (the angle between vectors $\mathbf{r}_\mathrm{i}$ and $\mathbf{F}_\mathrm{i}$), the surface element can be expressed as $dA = r_i^2 d\beta d\gamma / \cos\alpha$. So the stress $\sigma = F_i / dA = dQn_m P / (cdA)$, where F_i indicates the total force of all rays.

When the force doesn't distribute symmetrically, it results in a torque which will drive the particle to rotate in an optical trap until the torque is zero at appropriate orientation. For an ellipsoid, the total torque meets $\mathbf{T} = \sum_i \mathbf{r}_i \times \mathbf{F}_i$. While the ellipsoid locates in an arbitrary orientation, the torque can be calculated with rotating coordinate system as mentioned above.

3. Results

The filled state can be described by $\xi = \omega_0 / R_{obj}$. Without detailed explain, the beam is random polarization and Gaussian beam with $\xi = 1$. Some parameters in below calculation are the same, $R_{obj} = 3\,mm$, $P = 10\,mW$, the depth $z_{cg} = -10\,\mu m$, NA is 1.25, refractive index $n_{particle} = 1.59$, $n_{water} = 1.33$, $n_{glass} = 1.51$. Taking a sphere with $r_{bead} = 3\,\mu m$ as a reference, the fractional radii can be express as $\varepsilon_x = a / r_{bead}$, $\varepsilon_y = b / r_{bead}$ and $\varepsilon_z = c / r_{bead}$.

3.1. Torque of an Ellipsoid

An ellipsoid located in an arbitrary orientation is shown in Fig. 1(d). When the semi-principal axes are parallel to coordinate axes, $\beta_{axis} = 0$ and $\gamma_{axis} = 0$, the torque of the ellipsoid is zero. The torque of the ellipsoid with $\beta_{axis} = 0$ is calculated in Tab.1. In the case of the ellipsoid with $\varepsilon_x = 1$, $\varepsilon_y = 2$ and $\varepsilon_z = 3$, the torque has only component of T_y while $0 < \gamma_{axis} < \pi/2$, and $T_y < 0$. It indicates that the torque will rotate the ellipsoid to the orientation of $\gamma_{axis} = 0$. While $\gamma_{axis} > \pi/2$, $T_y > 0$, it indicates that the torque will rotate the ellipsoid to the

#167000 - $15.00 USD Received 18 Apr 2012; revised 23 May 2012; accepted 5 Jun 2012; published 19 Jun 2012

orientation of $\gamma_{axis} = \pi$. However, $\gamma_{axis} = 0$ and $\gamma_{axis} = \pi$ are in the same orientation. Though the torque is zero while $\gamma_{axis} = \pi/2$, the ellipsoid in this orientation is not stable, because the torque induced by very little deviation of γ_{axis} will rotate ellipsoid to enlarge this deviation. In the case of the ellipsoid with $\varepsilon_x = 3$, $\varepsilon_y = 2$ and $\varepsilon_z = 1$, the torque of the ellipsoid is zero while $\gamma_{axis} = 0$ and $\gamma_{axis} = \pi$, but very little deviation of γ_{axis} will induce the particle to speed up this deviation. Finally the ellipsoid is stable at $\gamma_{axis} = \pi/2$. So the torque will automatically regulate orientation of the ellipsoid to long axis parallel to optic axis (*z*-axis).

Table 1. Torque of an Ellipsoid While $\beta_{axis} = 0$

$\varepsilon_x = 1$, $\varepsilon_y = 2$, $\varepsilon_z = 3$		$\varepsilon_x = 3$, $\varepsilon_y = 2$, $\varepsilon_z = 1$	
γ_{axis}	$T_y(N\cdot\mu m)$	γ_{axis}	$T_y(N\cdot\mu m)$
00	0	00	0
π/6	−1.14	π/6	0.53
π/3	−0.53	π/3	1.14
π/2	0	π/2	0
2π/3	0.53	2π/3	−1.14
5π/6	1.14	5π/6	−0.53

3.2 Stress of an ellipsoid

The grids composed of β and γ on an ellipsoid surface are divided into 64×80. Figure 2 indicates the stress distribution of a sphere ($\varepsilon_x = \varepsilon_y = \varepsilon_z = 1$) and an ellipsoid ($\varepsilon_x = 1$, $\varepsilon_y = 2$, $\varepsilon_z = 3$) in an optical trap with spherical aberration. The stress of the sphere at a specific γ has the same value for different β. For a sphere at original point *O*, the stress distribution is severe at a narrow region (160°-180°) with large peak at $\gamma = 165°$ as this surface (the front surface, 90°-180°) suffers incident focused rays at first. Since the dielectric sphere is similar to a lens, the refractive rays across on the front surface are further deflected. As a result, the striking region of incident rays on the back surface (0°-90°) is larger than that on the front surface. Furthermore, the rays striking on the back surface are diffused due to the spherical aberration of particle. So the stress distribution on the back surface is low and gentle.

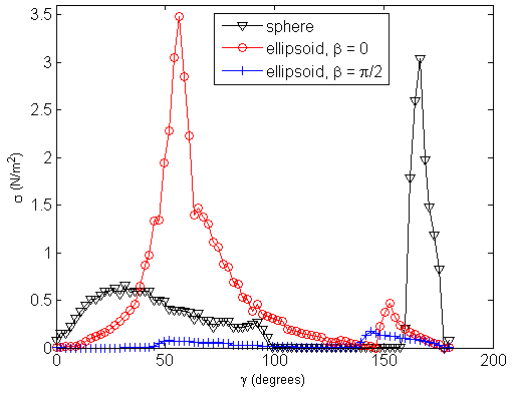

Fig. 2. Stress distribution of a sphere and an ellipsoid.

While an ellipsoid is at original point *O* andits longest axis is parallelto optic axis, the stress σ varies with orientation β as an ellipsoid is not symmetric for revolution. While $\beta = 0$ (in *x*-*z* plane) in Fig. 2, stress σ is relatively strong on the back surface with a large peak at

#167000 - $15.00 USD Received 18 Apr 2012; revised 23 May 2012; accepted 5 Jun 2012; published 19 Jun 2012

γ = ~55°, but it is weak on the front surface. However, the overall distribution of stress is very weak on both front and back surfaces while $\beta = \pi/2$ (in y-z plane). Those differences are originated from the astigmatism when rays go across an aspheric surface of ellipsoid. As a whole, the stress distribution on the surface of small fractional radius (along x-axis, $\beta = 0$) will stronger than on the surface of large fractional radius (along y-axis, $\beta = \pi/2$). For soft particles such as red blood cells or vesicles, the surface of small fractional radius can be expanded more easily due to high stress.

3.3 Optical Forces on an Ellipsoid

As mentioned above, the long axis parallel to z-axis is the most stable state for an ellipsoid. Here taking an ellipsoid of $\varepsilon_x = 1$, $\varepsilon_y = 2$ and $\varepsilon_z = 3$ as an example, we analyze what factors affect the optical forces.

In RO model the optical forces on a sphere affected by polarization [21]. For an ellipsoid, the optical forces at coordinate axes are calculated for random polarization and x-polarization in Fig. 3. For the different polarizations, there are small differences in all optical forces. With comparison of the transverse maximum restoring forces ($|Q_{tr}|_{max}$) in Fig. 3(a), however, the force at x-axis is much lower than at y-axis whether the beam is polarized or not. So does axial pushing force ($Q_z > 0$) in Fig. 3(b) while the ellipsoid has transverse displacement. Figure 3(c) shows the axial force at z-axis, there is a very small difference near $Q_z = 0$ in the two cases of polarization. So the polarization affects the forces very little compared with deformable ratio.

For a trapped bead with transverse displacement, the axial pushing force affects axial equilibrium and induces to axially escape before the bead arriving at the maximum transverse displacement [21, 31, 32]. So the maximum force of experimental measurement is lower than the calculated force. If we measure the maximum force at y-axis, the pushing force rapidly increases with displacement increasing (see Fig. 3(b)).Thus, the experimental value is lower than theoretical value. While at x-axis, since the pushing force is always low, the experimental value is close to theoretical value. So the differences of transverse forces at x- and y-axes will be reduced.

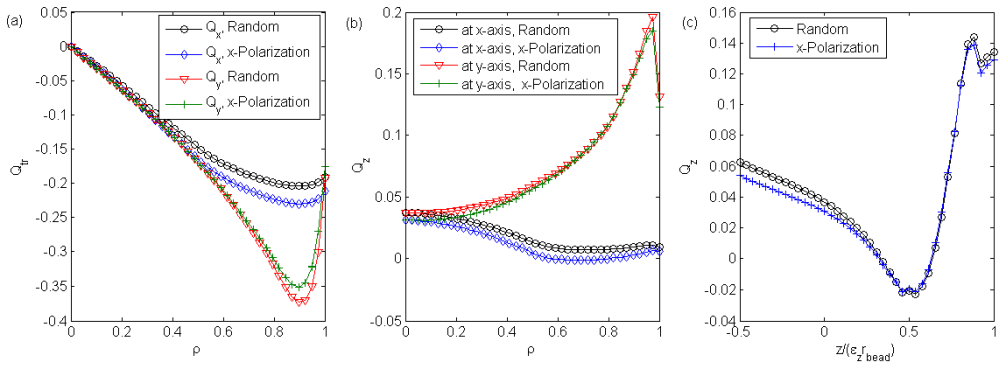

Fig. 3. Optical forces of an ellipsoid with polarized beams. Normalized transverse displacement $\rho = D_i / (\varepsilon_i r_{bead})$, the index i is x or y. (a) Transverse forces in transverse directions; (b) Axial pushing force in transverse directions; (c) Axial force at z-axis.

In Fig. 3(c), the spherical aberration weakens the axial restoring force. To our knowledge, a ring beam can enhance the axial restoring force and improves the axial stability [25]. Figure 4 shows ring beam profiles with $n = 1$ and the forces on an ellipsoid. In Fig. 4(a), ring beam profiles are the dark-hollow distribution, and the location of peaks is far away from optic axis

#167000 - $15.00 USD Received 18 Apr 2012; revised 23 May 2012; accepted 5 Jun 2012; published 19 Jun 2012

with increasing of ξ. While ξ = 0.4 (in Fig. 4(b)), $Q_z > 0$ in axial direction indicates that the ellipsoid can't be trapped. As ξ increases, the axial restoring force is enhanced. Owing to beam apodized by the objective entrancing aperture, however, there is no distinct difference at the axial restoring force for $\xi = 0.6$ and $\xi = 0.8$. From Figs. 4(c) to 4(f), the transverse and pushing forces are both weakened with increasing of ξ. Under the same condition of ξ, $|Q_y|_{max}$ is also stronger than $|Q_x|_{max}$. This tendency is determined by the deformable ratio of an ellipsoid and not related with beam profile. The ring beam with large ξ not only improves axial stability but also enlarge the maximum transverse displacement. Compared with a Gaussian beam and ring beams in Fig. 4, the optical trap formed by a ring beam ($n = 1$, $\xi = 0.6$) has better axial stability and large transverse forces, and this parameters are used in the below calculation.

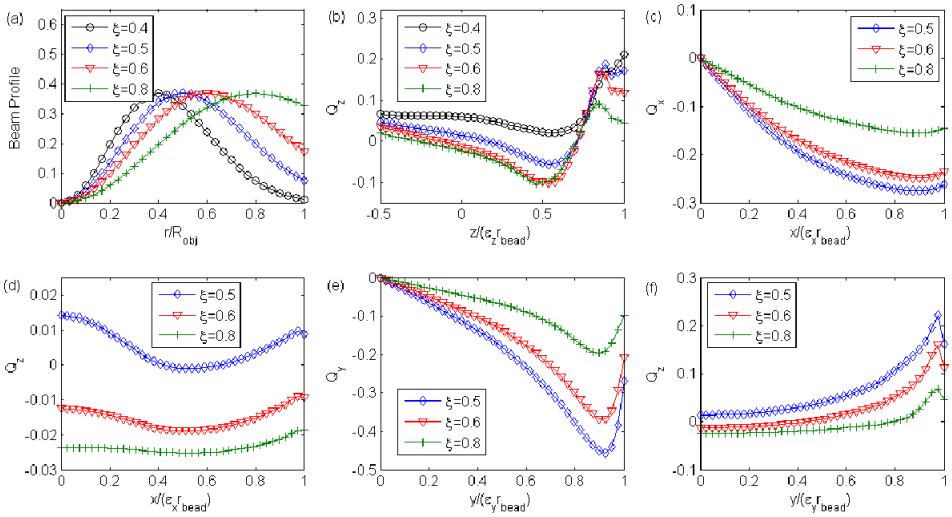

Fig. 4. Ring beam profiles ($n = 1$) and optical forces on an ellipsoid in an optical trap formed by ring beams. (a) Beam profiles of intensity on the objective entrancing aperture; (b) Axial force at z-axis; Transverse (c) and axial (d) forces at x-axis; Transverse (e) and axial (f) forces at y-axis.

While an ellipsoid departs laterally from trap center, the non-symmetric stress and torque will propel the particle's semi-major axis to incline in the x-z plane (type-A) or in y-z plane (type-B), as shown in Fig. 1(d). As the inclined angle γ_{axis} varies, the corresponding torques are shown in Tab. 1, and the optical forces in the two cases are shown in Fig. 5. For type-A (in Fig. 5(a)), $|Q_x|_{max}$ increases within creasing of γ_{axis}, and its corresponding location is far away from the trap center. Thus, the experimental maximum displacement at x-axis for inclined ellipsoid will be beyond in the case of γ_{axis} = *0*. For type-B (in Fig. 5(b)), however, $|Q_y|_{max}$ decreases with increasing of γ_{axis}, and its corresponding location changes very little. If we assay the transverse forces, the maximum force at y-axis is weakened but enhanced at x-axis due to the inclined pose of an ellipsoid. While the ellipsoid moves along axes at appropriate inclined angle, the gap between $|Q_x|_{max}$ and $|Q_y|_{max}$ can be small. From Figs. 5(a) to 5(b), the maximum transverse forces on an ellipsoid are both larger than those forces on a sphere. For axial force at *z*-axis, there is no difference in two cases with same inclined angle. In Fig. 5(c), the axial restoring force decreases with increasing of γ_{axis}, this will weaken the axial stability, as mentioned in section 3.1.

#167000 - $15.00 USD Received 18 Apr 2012; revised 23 May 2012; accepted 5 Jun 2012; published 19 Jun 2012

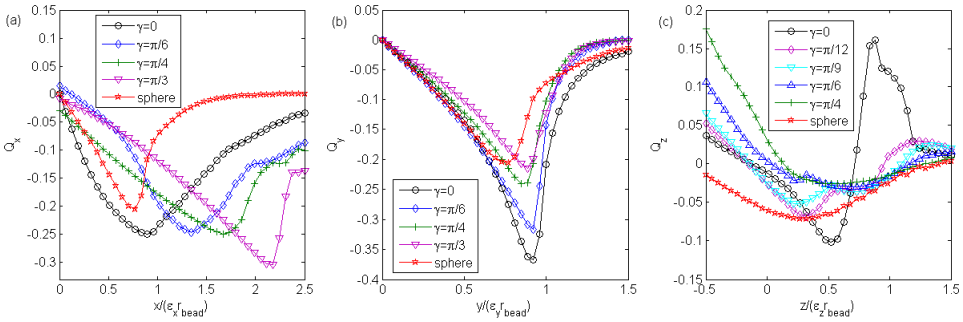

Fig. 5. Optical forces of an inclined ellipsoid. (a) Type-A; (b) Type-B; (c) At z-axis.

4. Summary

In this paper, we analyze optical forces on an ellipsoid in an optical trap with spherical aberration using vectorial ray tracing. For the ellipsoid, the torque will automatically regulate its orientation and high stress appears on the surface of small fractional radius. For a soft particle, the high stress induces to expand more easily. A ring beam of $\xi > 0.4$ can improve axial trapping stability, but the appropriate beam profile does not weaken the maximum transverse optical forces, such as $\xi = 0.6$ ($n = 1$). Due to the effect of shape size, $|Q_y|_{max}$ is much larger than $|Q_x|_{max}$ in theoretical calculations for both a Gaussian and ring beams. while an ellipsoid departs laterally from trap center, $|Q_x|_{max}$ will be enhanced and $|Q_y|_{max}$ will be weakened by inclined pose. Thus, the measurement of force depends on the shape size and orientation. To manipulate a living cell, the laser power of an optical trap should be reduced as low as possible for avoiding the damage from laser. However, the optical forces and axial stability will be weakened at the same time. For the optical trap formed by an appropriate ring beam, since the maximum transverse displacement can be enlarged and the axial stability is improved, the maximum transverse forces are enhanced. Thus, this optical trap is more appropriate to trap cells directly.

Acknowledgments

This work is supported by National Natural Science Foundation of China (31100555, 20974107 and 21073174), Chinese Universities Scientific Fund (WK2030020016, WK2030380002) and China Postdoctoral Science Foundation (20110490830).

#167000 - $15.00 USD Received 18 Apr 2012; revised 23 May 2012; accepted 5 Jun 2012; published 19 Jun 2012